

Single Point, Full Mask: Velocity-Guided Level Set Evolution for End-to-End Amodal Segmentation

Zhixuan Li¹, Yujia Liu^{2,3,4}, Chen Hui⁵, Weisi Lin^{1*}

¹College of Computing and Data Science, Nanyang Technological University, Singapore

²School of Computer Science, Peking University, Beijing, China

³National Key Laboratory for Multimedia Information Processing, Peking University, Beijing, China

⁴National Engineering Research Center of Visual Technology, Peking University, Beijing, China

⁵Nanjing University of Information Science and Technology, China

Abstract

Amodal segmentation aims to recover complete object shapes, including occluded regions with no visual appearance, whereas conventional segmentation focuses solely on visible areas. Existing methods typically rely on strong prompts, such as visible masks or bounding boxes, which are costly or impractical to obtain in real-world settings. While recent approaches such as the Segment Anything Model (SAM) support point-based prompts for guidance, they often perform direct mask regression without explicitly modeling shape evolution, limiting generalization in complex occlusion scenarios. Moreover, most existing methods suffer from a black-box nature, lacking geometric interpretability and offering limited insight into how occluded shapes are inferred. To deal with these limitations, we propose VELA, an end-to-end VELocity-driven Level-set Amodal segmentation method that performs explicit contour evolution from point-based prompts. VELA first constructs an initial level set function from image features and the point input, which then progressively evolves into the final amodal mask under the guidance of a shape-specific motion field predicted by a fully differentiable network. This network learns to generate evolution dynamics at each step, enabling geometrically grounded and topologically flexible contour modeling. Extensive experiments on COCOA-cls, D2SA, and KINS benchmarks demonstrate that VELA outperforms existing strongly prompted methods while requiring only a single-point prompt, validating the effectiveness of interpretable geometric modeling under weak guidance. The code will be publicly released.

1 Introduction

The conventional visible segmentation task focuses solely on observable areas and is typically formulated as a pixel-wise classification problem, without inferring the shapes of occluded regions. In contrast, the amodal segmentation task aims to predict complete object masks, including both visible and occluded parts, by reasoning about the full object shape from the available visual cues. Despite its challenges, amodal segmentation is crucial in real-world applications like weather forecasting (Zhao et al. 2020; Fan et al. 2025), urban mapping (Guo et al. 2018; Li et al. 2010b), and land-use monitoring (Mas and González 2015; Johnson and Ma 2020). Environmental occluders such as vegetation, terrain,

or atmospheric effects often occlude key areas in aerial images. Recovering amodal object shapes provides complete and reliable spatial information of surface geometry for climate analysis.

Existing state-of-the-art amodal segmentation methods (Zhan et al. 2020; Ling et al. 2020; Zheng et al. 2021; Nguyen and Todorovic 2021; Liu et al. 2025) mostly rely on strong input prompts, such as visible masks (Zhan et al. 2020; Ling et al. 2020; Zheng et al. 2021; Nguyen and Todorovic 2021; Gao et al. 2023; Zhan et al. 2024) or bounding boxes (Liu, Li, and Jiang 2024; Liu et al. 2025), to guide the prediction of amodal masks covering occluded regions. As shown in Fig.1 (a), while these methods have achieved notable performance, obtaining such strong prompts is often impractical or expensive in real-world scenarios, significantly limiting the applicability and generalizability of these approaches. Recent models like the Segment Anything Model (SAM) (Kirillov et al. 2023; Xiong et al. 2024; Ke et al. 2024) have introduced support for point-based prompts, offering a more lightweight form of guidance. However, as shown in Fig.1 (b), these approaches typically perform direct mask prediction from these sparse point-based prompts without an explicit mechanism to reason about the shape of occluded regions. As a result, their generalization ability remains limited in complex occlusion scenarios, where point prompts alone provide insufficient guidance for accurately inferring the complete amodal mask.

Another key limitation of existing approaches (Zhan et al. 2024; Tai et al. 2025; Li et al. 2023a,c; Chen et al. 2023) lies in their black-box nature, which lacks geometric interpretability in the amodal mask prediction process. Specifically, most existing methods adopt CNN-based (Zhang et al. 2019; Hu et al. 2019; Qi et al. 2019; Follmann et al. 2019; Zhan et al. 2020; Xiao et al. 2021; Li et al. 2022b, 2023b) or Transformer-based (Tran et al. 2022; Li et al. 2023a; Tran et al. 2024; Li et al. 2025) architectures that treat amodal mask prediction as a direct regression task, without modeling the underlying morphological processes involved in shape segmentation. Consequently, these models offer little transparency into the internal reasoning behind their predictions, providing limited understanding of how occluded regions are inferred. This absence of explicit geometric reasoning not only limits the interpretability of the model’s predictions but also makes it difficult to analyze or improve

*Corresponding author.

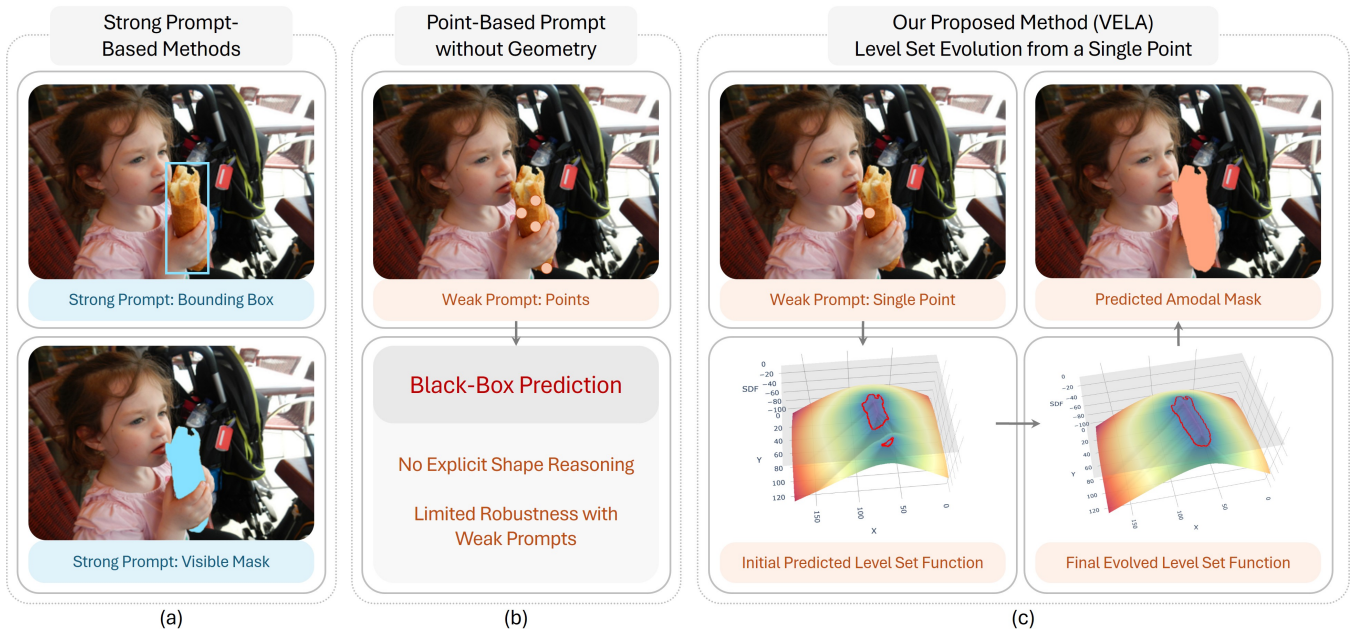


Figure 1: Comparison of amodal segmentation paradigms. (a) Conventional methods rely on strong prompts like bounding boxes or visible masks. (b) Recent approaches support point prompts but directly regress masks without explicit shape reasoning, resulting in limited robustness under complex occlusions. (c) VELA introduces explicit shape evolution via Level Set, effectively exploiting a single-point prompt for interpretable amodal segmentation.

model performance, especially in scenarios involving complex occlusions where understanding how the model reasons about fine-grained shapes is crucial for reliable prediction. Motivated by these limitations, we pose the following question: *is it possible to achieve high-quality amodal segmentation using only a weak prompt like a single point by fully leveraging a geometrically interpretable approach?*

To this end, we propose a novel approach named **VELA**, a **VELOCITY**-driven Level-set Amodal segmentation method, performing amodal segmentation via Level Set evolution with only a *single point* as input prompt, as shown in Fig.1 (c). Specifically, we begin by embedding the point prompt, which then interacts with the extracted image features to generate an initial level set function, representing the starting state of the object’s amodal mask. This initial function is then progressively updated through a guided evolution process to expand toward the final high-quality amodal mask. To enable precise and adaptive guidance during this evolution, we design a fully differentiable network that learns to predict a shape-specific velocity field, which drives the contour evolution at each step. This velocity prediction network dynamically generates the up-to-date velocity field based on the current state of the evolving contour, providing context-aware guidance that continuously steers the contour toward the complete amodal shape effectively.

This evolution process simulates the gradual expansion of the object’s boundary with the step-by-step guidance generated based on contour status and learned prior knowledge to evolve toward the target shape. In contrast to conventional approaches that directly predict the final mask in a single

step, our method models segmentation as a geometrically grounded and iterative process. This step-wise evolution not only enables more interpretable shape reasoning but also provides greater flexibility in handling complex occlusions and diverse object geometries. This is thanks to the Level Set paradigm’s inherent ability to explicitly represent and continuously evolve object contours in a geometrically interpretable and topologically flexible manner. Building upon the unique characteristics of our Level Set-based evolution, VELA introduces a novel paradigm for weakly prompted amodal segmentation. Moreover, the end-to-end framework allows adaptive modeling of diverse object shapes and occlusion patterns, alleviating limitations of prior black-box approaches with better transparency.

We extensively evaluate VELA on amodal segmentation benchmarks, including COCOA-cls, D2SA, and KINS. Results show that our weakly prompted Level Set-based approach outperforms strong-prompt methods, demonstrating the effectiveness of geometry-aware modeling.

Our contributions are summarized as follows: (1) We propose VELA, which, to the best of our knowledge, is the first amodal segmentation method that leverages Level Set evolution with point-based prompting. VELA achieves high-quality amodal segmentation with only a *single point* as input, reducing reliance on strong prompts like visible masks or boxes. (2) We introduce a fully differentiable framework that learns a shape-specific velocity field to explicitly guide the contour evolution process, enabling geometrically grounded and interpretable mask prediction. (3) We demonstrate that our method achieves well performance on amodal

segmentation datasets with the weak prompt, showing its generalization capability in complex occlusion scenarios.

2 Related Work

2.1 Amodal Segmentation

Since the amodal segmentation task proposed by (Li and Malik 2016), various approaches have been developed from different perspectives. Several approaches (Zhang et al. 2019; Hu et al. 2019; Qi et al. 2019; Xiao et al. 2021; Tran et al. 2022; Li et al. 2023a) are designed based on existing CNN-based or Transformer-based instance segmentation frameworks to tackle the amodal segmentation problem using only the input image. Meanwhile, many approaches (Zhan et al. 2020; Ling et al. 2020; Zheng et al. 2021; Nguyen and Todorovic 2021; Gao et al. 2023; Liu, Li, and Jiang 2024) reformulate the task as predicting the amodal mask from the image and additional prompts, such as visible or amodal bounding boxes, or visible masks. However, these strong prompts, especially bounding boxes and visible masks of target objects, are often impractical or costly to obtain in real-world scenarios. Such high demands on user input reduce the practicality of these methods and limit their ability to generalize to diverse scenarios, particularly in interactive applications.

To this end, in this paper, we investigate point-based weak prompts as guidance for amodal mask segmentation, thereby alleviating the dependence on strong yet difficult-to-obtain prompts. A natural solution is to leverage recent popular models, such as the Segment Anything Model (SAM), which are designed to accept point-based prompts as input. However, SAM focuses on visible mask segmentation with a direct prediction strategy and lacks explicit reasoning for occluded regions, which limits its ability to infer complete amodal masks, especially when only sparse point prompts are available that offer only coarse guidance of the visible parts of target objects. This motivates the need to explore how high-quality amodal segmentation can be achieved using only point-based prompts effectively.

2.2 Level Set Methods for Segmentation

Level set methods offer a powerful framework for image segmentation by implicitly encoding object boundaries as zero-level contours of higher-dimensional functions. Their capacity to represent arbitrary shapes and topological changes, such as merging and splitting, makes them particularly appealing for modeling complex object structures. Traditional approaches (Caselles, Kimmel, and Sapiro 1997; Kass, Witkin, and Terzopoulos 1988; Malladi, Sethian, and Vemuri 2002) typically focus on minimizing hand-crafted energy functions that capture low-level appearance cues, suffering from sensitivity to initialization and limited generalization ability.

To address these limitations, recent methods (Kim and Ye 2019; Homayounfar et al. 2020; Li et al. 2022a) have integrated the level set with deep learning frameworks. Some methods (Ngo and Carneiro 2013; Wang et al. 2019) improve initialization by using networks to predict coarse masks, edge probability maps, or contour priors

that serve as starting level-set functions. And several methods utilize the level set from different aspects, including for post-processing for semi-supervised segmentation (Tang et al. 2017), integrating in the loss function for shape regularization (Hu et al. 2017), and to denoise edge annotations (Acuna, Kar, and Fidler 2019).

Considering there are no existing methods exploring the level set framework for amodal segmentation, especially under point-based weak prompts, we propose VELA to learn and generate the shape-specific velocity field dynamically for explicitly guiding the evolution process.

3 Methodology

In this section, we present the proposed method, VELA. We begin by defining the task of amodal segmentation. We then provide a detailed overview of the VELA architecture, followed by an explanation of the shape-specific velocity generation network. Next, we describe the velocity-guided amodal shape evolution framework. Finally, we introduce the learning objective used for end-to-end training.

3.1 Task Definition

Given an input image I and an optional prompt P , the goal of amodal segmentation is to predict the complete amodal mask \hat{M}_a of the target object. The prompt P can take various forms, such as bounding boxes, masks, or points. In this work, we focus on point-based prompts, which offer coarse but efficient guidance for localizing the object to be segmented.

3.2 Overall Architecture

The proposed VELA consists of the following modules, as illustrated in Fig. 2. First, we introduce feature extraction from inputs. Specifically, the backbone network processes the input image I to extract the global feature representation F of the entire scene. Simultaneously, the prompt encoder takes the point prompt P as input and produces a sparse embedding e_P , which encodes coarse localization information about the target object to be segmented. A *single point* prompt for the target object can provide sufficient guidance for effective amodal segmentation, while VELA also supports multiple point prompts if available.

Next, we introduce the evolution process guided by shape-specific velocity fields. A mask decoder first predicts the initial level set function ϕ_0 , which is then iteratively evolved over T steps to produce the final level set function ϕ_T . At each step $i \in \{1, \dots, T-1\}$, the level set function ϕ_i is updated using a dynamically generated, shape-specific velocity field that provides adaptive guidance to progressively deform ϕ_i toward the target amodal mask. After T steps of evolution, the final level set function ϕ_T is converted into a binary mask by thresholding at 0, resulting in the predicted foreground amodal mask.

3.3 Level Set Function Initialization

The level set function is initialized by predicting ϕ_0 using a mask decoder, which takes the global image feature F and the sparse prompt embedding e_P as inputs. For a 2D binary

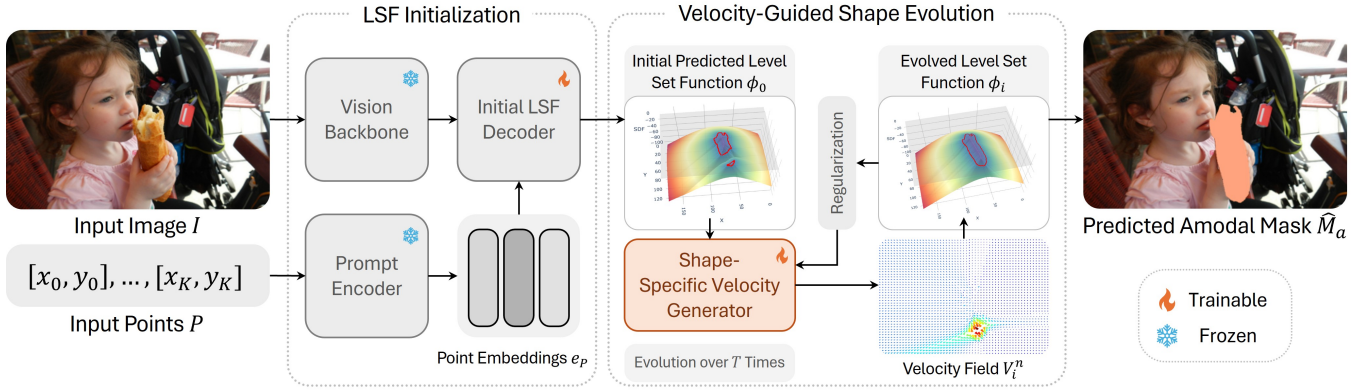


Figure 2: Overall architecture of the proposed VELA. (a) Level Set Function (LSF) Initialization: Given an input image I , the Vision Backbone extracts global image features, while the Prompt Encoder processes the point-level prompt P to generate point embeddings e_P that encode coarse localization of the target object. The Initial LSF Decoder then predicts the initial level set function ϕ_0 using both the image features and point embeddings. (b) Velocity-Guided Shape Evolution: Starting from ϕ_0 , the shape evolves over T steps. At each step i , the current level set function ϕ_i is fed into the Shape-Specific Velocity Generator to dynamically produce a velocity field V_i^n , which guides the contour’s deformation towards the final shape. The updated ϕ_{i+1} is then regularized and used for the next step. After T steps, the final level set function ϕ_T is thresholded to obtain the predicted amodal mask \hat{M}_a . Best viewed in color.

Algorithm 1: Velocity-Guided Level Set Evolution

Input: Initial level set function ϕ_0 , number of steps T , time step dt

Components: Velocity predictor $\mathcal{F}_v(\cdot)$, distance regularizer $\mathcal{R}(\cdot)$

Output: Final evolved level set function ϕ_T

- 1: Initialize $\phi \leftarrow \phi_0$
 - 2: **for** $i = 0$ to $T - 1$ **do**
 - 3: Predict normal velocity $V_i^n \leftarrow \mathcal{F}_v(\phi)$
 - 4: Update $\phi \leftarrow \phi - dt \cdot V_i^n$
 - 5: Apply regularization: $\phi \leftarrow \phi + \mu \cdot \mathcal{R}(\phi)$
 - 6: **end for**
 - 7: **return** $\phi_T \leftarrow \phi$
-

mask M that contains a 2D curve \mathcal{C} of the target object, the level set function ϕ provides a higher-dimensional implicit representation of M . Specifically, ϕ is a 3D surface whose zero level set corresponds to the object boundary curve \mathcal{C} in the 2D mask M . Here, we define background regions as negative and foreground regions as positive. Accordingly, the binary mask M can be obtained by thresholding the level set function ϕ at zero, retaining values greater than zero as the foreground. We can formulate the aforementioned correspondence as follows:

$$M(x, y) = \begin{cases} 1, & \text{if } \phi(x, y) > 0 \\ 0, & \text{otherwise} \end{cases} \quad \text{with } \mathcal{C} = \partial M \quad (1)$$

Here, x and y represent the 2D spatial coordinates of the image, and ∂ denotes the boundary operator. Accordingly, $\mathcal{C} = \partial M$ defines the object contour corresponding to the boundary of the binary mask M .

In our design, the predicted initial level set function ϕ_0 corresponds to the mask of visible regions for the target object, since the input point-based point only provides very coarse guidance to the visible part of the object. Compared to the traditional approach of level set, our initialization is predicted by the network in an end-to-end approach.

3.4 Velocity-Guided Shape Evolution

The proposed VELA is designed to fully leverage the information provided by the sparse prompt to achieve high-quality amodal segmentation through a geometrically interpretable approach. A velocity-guided shape evolution process is introduced to drive the morphological transformation of the level set function from the initial state ϕ_0 , corresponding to the predicted visible mask, toward the final state ϕ_A , representing the ground-truth amodal mask M_a . The complete evolution procedure is outlined in Alg. 1.

Specifically, the initial level set function ϕ_0 is evolved over T steps to expand the initial contour of the visible mask toward the target amodal mask, which typically encompasses a larger region than the visible mask. Based on the level set theory, for step $i \in \{0, \dots, T - 1\}$, the progressively updating process can be formulated as:

$$\phi_{i+1} = \phi_i + dt \frac{\partial \phi}{\partial t}, \quad (2)$$

where dt denotes the time step, representing the time amount for the contour to move per step, and $\frac{\partial \phi}{\partial t}$ represents the temporal derivative of the level set function, governing its deformation over time. In classical level set theory, the contour evolves along its normal direction, and the update term is defined as:

$$\frac{\partial \phi}{\partial t} = -V_i^n \|\nabla \phi\|, \quad (3)$$

where V_i^n denotes the predicted normal velocity field at step i , which controls the speed of evolution along the normal direction, and $\|\nabla\phi\|$ is the gradient magnitude that enforces evolution along the normal direction.

To simplify the computation and ensure numerical stability, we apply a regularization term after each evolution step to maintain the level set function ϕ_i as a signed distance function (SDF), which keeps $\|\nabla\phi\|$ close to 1 throughout the evolution. Under this condition, the evolution equation can be simplified by treating the gradient norm as nearly constant and close to 1. As a result, Eqn. 3 becomes:

$$\frac{\partial\phi}{\partial t} = -V_i^n, \quad (4)$$

leading to a simplified update rule:

$$\phi_{i+1} = \phi_i - dt \cdot V_i^n. \quad (5)$$

This formulation allows the evolving contour to be directly guided by the predicted scalar velocity field V_i^n , while the distance regularization ensures that the geometric meaning of the level set function is preserved throughout the evolution process.

To implement this, we adopt a distance regularization term $\mathcal{R}(\phi)$ inspired by the double-well potential in DRLSE (Li et al. 2010a), which encourages $\|\nabla\phi\|$ to stay close to 1. Specifically, at each step, we add a regularization update:

$$\phi_{i+1} = \phi_i - dt \cdot V_i^n + \mu \cdot \mathcal{R}(\phi_i), \quad (6)$$

where μ is a weighting factor. This regularization supports maintaining the signed distance property of ϕ , thereby enabling the approximation that the gradient norm remains close to 1 throughout the evolution.

Finally, the amodal segmentation mask is obtained by applying a zero threshold to the final level set function ϕ_T , with the foreground amodal mask M_a defined as $\{(x, y) \mid \phi_T(x, y) > 0\}$.

Shape-Specific Velocity Generation. To enable accurate and interpretable evolution of the level set function, we introduce the Shape-Specific Velocity Generator that dynamically predicts the normal velocity field V_i^n at each evolution step. Specifically, we employ a lightweight UNet architecture that takes the current level set function ϕ_i as input and outputs a scalar velocity map that guides the contour deformation. This predicted velocity field encodes the directional cues required to deform the current visible contour toward the final amodal shape, allowing the model to learn shape-aware motion patterns conditioned on the evolving mask geometry dynamically.

3.5 Training Objective

To supervise the evolution of the level set function toward the desired amodal shape, we define a loss that provides step-wise guidance during training. For each evolved level set function ϕ_i at step i , we apply a smooth approximation of the Heaviside function $H(\phi_i)$ to obtain a differentiable soft mask, which maps positive values to foreground and negative values to background, enabling end-to-end learning. We

then compute a binary cross-entropy (BCE) loss between the soft prediction and the ground-truth amodal mask M_a :

$$\mathcal{L}_{\text{evo}} = \sum_{i=0}^{T-1} \text{BCE}(H(\phi_i), M_a), \quad (7)$$

This cumulative loss encourages the model to learn meaningful velocity fields that progressively deform the evolving contour toward the complete amodal mask.

4 Experiments

To evaluate the effectiveness of the proposed VELA, we conduct experiments on three challenging datasets. Compared with existing methods, VELA achieves state-of-the-art performance. We illustrate the comparison both quantitatively and qualitatively. Finally, extensive ablation studies are conducted to validate the design of VELA.

4.1 Datasets and Evaluation Metrics

Datasets. We conduct experiments on three publicly available datasets to evaluate the performance of VELA. Specifically, first, the COCOA-cls (Follmann et al. 2019) dataset contains 3,501 images and 10,592 ground-truth masks across 80 categories, which is constructed based on the famous COCO (Lin et al. 2014) dataset. The COCOA-cls dataset serves as a crucial benchmark due to its diverse and representative daily life scenarios. Second, the D2SA (Follmann et al. 2019) dataset is designed for the shopping scenario, where self-checkout systems are commonly used. With 5,600 images and 28,720 ground-truth masks in 60 categories provided, the D2SA dataset can effectively examine the amodal segmentation ability of methods with its intrinsic occlusions constructed by overlapping merchandise. Finally, built upon the KITTI (Geiger, Lenz, and Urtasun 2012) dataset, the KINS (Qi et al. 2019) dataset comprises 7,474 and 7,517 images in the training and testing splits, respectively. It primarily captures street scenes, making it a valuable benchmark for assessing amodal segmentation performance in complex urban environments.

It is worth noticing that, for each dataset, all methods are trained on the same official training split and tested on the same official validation or testing split to ensure fairness. All experiments of VELA are conducted three times, and the average performance is reported to mitigate the impact of randomness.

Evaluation Metrics. Following (Gao et al. 2023), we adopt mean Intersection over Union (mIoU) as the evaluation metric, computed over two regions: the entire amodal mask and the occluded regions. These are denoted as $\text{mIoU}_{\text{full}}$ and mIoU_{occ} , respectively. Larger values indicate better performance.

4.2 Implementation Details

We implement our proposed VELA framework based on PyTorch (Paszke et al. 2019). VELA takes SAM2 (Ravi et al. 2024) as the base structure, whose pretrained weights are

Methods	Venue	Prompt	COCOA-cls (Val)		D2SA (Val)		KINS (Test)	
			mIoU _{full} ↑	mIoU _{occ} ↑	mIoU _{full} ↑	mIoU _{occ} ↑	mIoU _{full} ↑	mIoU _{occ} ↑
<i>Zero-shot Methods</i>								
SAM (Kirillov et al. 2023)	ICCV 2023	Mask	73.10	-	84.65	-	75.88	-
SDXL-Inpainting (Podell et al. 2024)	ICLR 2024	Mask	73.65	-	80.53	-	76.19	-
Pix2Gestalt (Ozguroglu et al. 2024)	CVPR 2024	Mask	79.08	-	81.82	-	81.45	-
<i>Fully-Supervised Methods</i>								
BCNet (Ke, Tai, and Tang 2021)	CVPR 2021	-	15.10	-	74.90	-	44.00	-
SLN (Zhang et al. 2019)	MM 2019	-	31.50	-	31.20	-	14.20	-
ORCNN (Follmann et al. 2019)	WACV 2019	-	57.60	-	74.10	-	55.10	-
Mask-RCNN (He et al. 2017)	ICCV 2017	-	63.85	-	74.62	-	60.13	-
A3D (Li et al. 2022b)	ECCV 2022	-	64.27	-	74.71	-	61.43	-
GIN (Li et al. 2023b)	TMM 2023	-	72.46	-	78.23	-	68.31	-
AISFormer (Tran et al. 2022)	BMVC 2022	-	72.69	13.75	86.81	30.01	81.53	48.54
PCNet (Zhan et al. 2020)	CVPR 2020	Mask	76.91	20.34	80.45	28.56	78.02	38.14
VRSP (Xiao et al. 2021)	AAAI 2021	-	78.98	22.92	88.08	35.17	80.70	47.33
SDAmodal (Zhan et al. 2024)	CVPR 2024	Mask	80.01	-	-	-	-	-
C2F-Seg (Gao et al. 2023)	ICCV 2023	Mask	80.28	-	89.10	-	82.22	-
VELA (Ours)	-	Point	80.68	25.00	89.96	39.41	83.06	50.29

Table 1: Comparison with state-of-the-art approaches on the COCOA-cls dataset (validation split), the D2SA dataset (validation split), and the KINS dataset (testing split). Metrics mIoU_{full} and mIoU_{occ} are employed and higher value indicates better performance. All zero-shot methods are first pretrained on a large-scale synthetic dataset proposed by (Ozguroglu et al. 2024) containing 873K images and then tested on the three datasets. For the prompt type, “Mask” refers to the visible mask of the target object, while “Point” indicates a single point located within the visible region of the target object.

used for initializing VELA. The optimizer for gradient descent is AdamW. For computing infrastructure, all experiments are conducted on a machine equipped with an AMD 9950X3D with 96 GB system memory, a NVIDIA 5090 (32GB) GPU, and the Windows 11 operating system. There are no data augmentation techniques employed in the experiments of VELA.

4.3 Comparison with State-of-the-art Methods

We compare the proposed VELA with state-of-the-art approaches, including both zero-shot and fully supervised methods. Specifically, zero-shot methods are pretrained on the large-scale Pix2Gestalt amodal segmentation dataset (Ozguroglu et al. 2024), which comprises approximately 873,000 synthetic images with simulated occlusions and corresponding ground-truth amodal masks. Fully-supervised methods, including VELA, are trained exclusively on the training splits of the three datasets, without utilizing any additional amodal segmentation data. Several methods use the visible mask of the target object as the input prompt, whereas VELA relies solely on a single point located within the visible region.

As shown in Tab. 1, VELA consistently outperforms all compared methods on both mIoU_{full} and mIoU_{occ}, achieving state-of-the-art performance. Compared to the zero-shot method, Pix2Gestalt, which is pretrained on a large-scale amodal segmentation dataset, VELA achieves gains of 1.6%, 8.14%, and 1.61% on the mIoU_{full} metric across the three benchmarks. Moreover, although the fully supervised method C2F-Seg performs strongly, VELA surpasses it on all three datasets. Remarkably, despite using only a sin-

Index	Evolution Steps T	COCOA-cls	D2SA	KINS
1	1	58.42	62.36	56.49
2	2	69.67	79.20	66.99
3	3	80.68	89.96	83.06
4	4	78.68	83.52	<u>80.58</u>
5	5	79.09	88.75	77.66
6	10	<u>79.75</u>	<u>89.65</u>	78.39

Table 2: Ablation study of the evolution steps.

gle point as the prompt, VELA obtains better results than methods that rely on visible mask-based prompts, demonstrating the effectiveness of our geometrically interpretable Level Set evolution, which progressively transforms the visible region into the complete amodal shape under learned velocity guidance.

Moreover, Fig. 3 shows qualitative results of VELA on the COCOA-cls dataset. We can observe that in all cases, VELA can predict high-quality amodal masks thanks to its explicit shape modeling via velocity-guided level set evolution. By evolving the object contour from a single-point prompted vision region, VELA effectively infers occluded regions in a geometrically interpretable manner, demonstrating robustness against complex occlusions and diverse object shapes.

4.4 Ablation Study

We conduct ablation studies on VELA to evaluate the effectiveness of its key components, including level set evolution steps, the number of input points, and the segmentation supervision strategy. Unless otherwise stated, all experiments

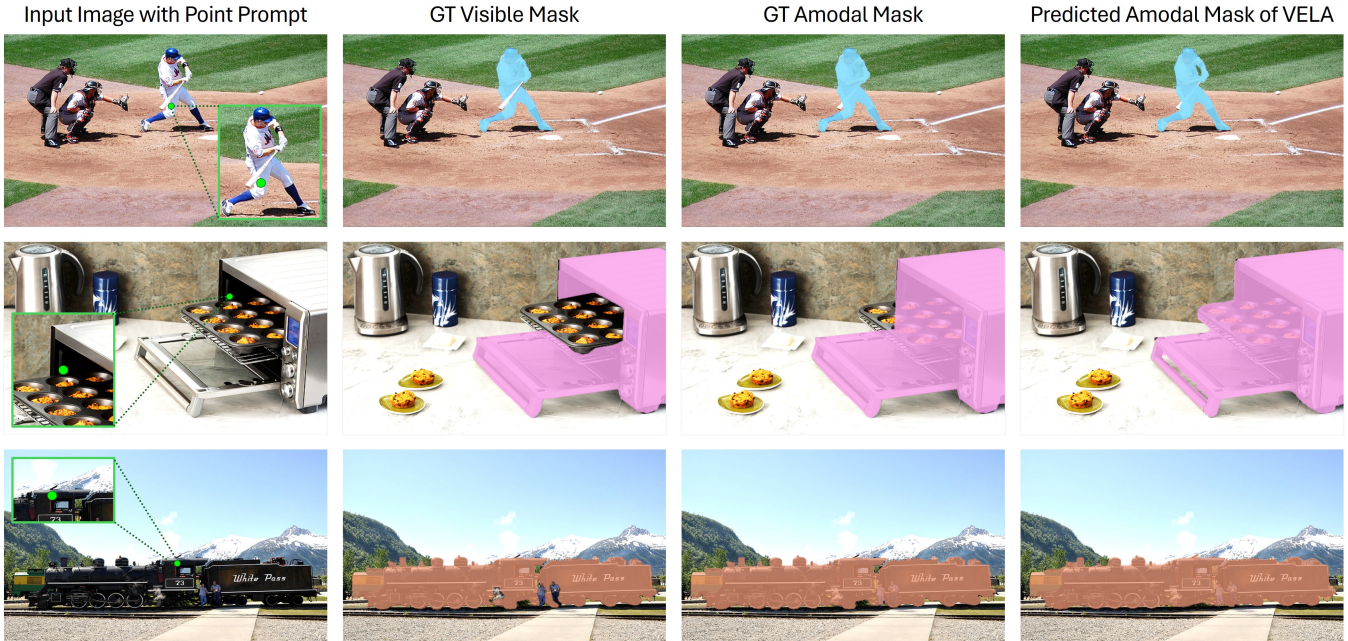


Figure 3: Visualization results of VELA. The green dot denotes the input point prompt. Best viewed in color.

Index	# Input Point(s)	COCOA-cls	D2SA	KINS
1	1	80.68	89.96	83.06
2	5	80.72	90.12	83.51
3	10	80.79	90.23	83.94
4	20	80.83	90.51	83.96
5	50	79.86	89.11	83.02

Table 3: Ablation study of the number of input points.

Index	Supervision Design	COCOA-cls	D2SA	KINS
1	Only final prediction	79.12	88.64	81.47
2	All evolved predictions	80.68	89.96	83.06

Table 4: Ablation study of the supervision design.

are conducted using three evolution steps and a single-point prompt. Results are reported using the $mIoU_{full}$ metric on the COCOA-cls, D2SA, and KINS datasets.

Effect of Evolution Steps T . As shown in Tab. 2, we evaluate the impact of varying the number of level set evolution steps T in VELA. The best performance is observed when $T = 3$. While fewer steps may limit occlusion recovery, a large number of steps can introduce mild contour smoothing or deformation, which may have a certain impact on the quality of predicted amodal masks.

Effect of Input Points Number. As shown in Tab. 3, we investigate the impact of using different numbers of point prompts. Increasing the number of input points brings modest improvements up to 20 points, but further increases offer little benefit and may introduce noise that affects perfor-

mance. Notably, VELA performs well even with a single-point prompt, demonstrating its ability to effectively utilize sparse guidance for high-quality amodal segmentation.

Effect of Supervision Design. We investigate two supervision strategies by either applying the loss only to the final evolved prediction or supervising all intermediate predictions throughout the evolution. As shown in Tab. 4, incorporating supervision at all steps consistently improves performance across datasets. This design enables step-wise supervision for the velocity field, allowing the model to refine the shape evolution more effectively and maintain stability throughout the process.

5 Limitations and Future Work

Although VELA provides interpretable shape evolution and performs well under sparse prompts, it currently applies a fixed number of evolution steps for all instances. This static setting may not be optimal for objects with varying occlusion levels or shape complexity. Future work could explore adaptive stopping criteria that adjust the number of evolution steps based on the characteristics of each instance, potentially improving both efficiency and segmentation quality.

6 Conclusion

In this paper, we present VELA, a velocity-guided level-set framework for amodal segmentation using weak, point-based prompts. Instead of relying on strong prompts or direct mask regression, VELA formulates segmentation as contour evolution, enabling explicit and interpretable shape modeling. A differentiable network predicts shape-specific velocity fields to guide the level set from an initial visible

contour to the full amodal mask. Experiments on COCOAcls, D2SA, and KINS show that VELA performs well with input point prompt, highlighting the potential of level set evolution as a principled approach to amodal segmentation.

References

- Acuna, D.; Kar, A.; and Fidler, S. 2019. Devil is in the edges: Learning semantic boundaries from noisy annotations. In *Proceedings of the IEEE/CVF Conference on Computer Vision and Pattern Recognition*, 11075–11083.
- Caselles, V.; Kimmel, R.; and Sapiro, G. 1997. Geodesic active contours. *International journal of computer vision*, 22(1): 61–79.
- Chen, J.; Niu, L.; Zhang, J.; Si, J.; Qian, C.; and Zhang, L. 2023. Amodal instance segmentation via prior-guided expansion. In *Proceedings of the AAAI Conference on Artificial Intelligence*, 1, 313–321.
- Fan, W.; Han, Y.; Shi, X.; Jin, Q.; Chen, Y.; and Qin, H. 2025. A distributed photovoltaic cluster power quantification model integrating ground-based cloud image segmentation technology and high-resolution weather forecasting technology. *Discover Artificial Intelligence*, 5(1): 85.
- Follmann, P.; König, R.; Härtinger, P.; Klostermann, M.; and Böttger, T. 2019. Learning to see the invisible: End-to-end trainable amodal instance segmentation. In *Proceedings of the IEEE/CVF Winter Conference on Applications of Computer Vision*, 1328–1336. IEEE.
- Gao, J.; Qian, X.; Wang, Y.; Xiao, T.; He, T.; Zhang, Z.; and Fu, Y. 2023. Coarse-to-fine amodal segmentation with shape prior. In *Proceedings of the IEEE/CVF International Conference on Computer Vision*, 1262–1271.
- Geiger, A.; Lenz, P.; and Urtasun, R. 2012. Are we ready for autonomous driving? the KITTI vision benchmark suite. In *Proceedings of the IEEE/CVF Conference on Computer Vision and Pattern Recognition*, 3354–3361. IEEE.
- Guo, Z.; Shengoku, H.; Wu, G.; Chen, Q.; Yuan, W.; Shi, X.; Shao, X.; Xu, Y.; and Shibasaki, R. 2018. Semantic segmentation for urban planning maps based on U-Net. In *IGARSS 2018-2018 IEEE international geoscience and remote sensing symposium*, 6187–6190. IEEE.
- He, K.; Gkioxari, G.; Dollár, P.; and Girshick, R. 2017. Mask R-CNN. In *Proceedings of the IEEE/CVF International Conference on Computer Vision*, 2961–2969.
- Homayounfar, N.; Xiong, Y.; Liang, J.; Ma, W.-C.; and Urtasun, R. 2020. Levelset r-cnn: A deep variational method for instance segmentation. In *Proceedings of the IEEE/CVF European Conference on Computer Vision*, 555–571. Springer.
- Hu, P.; Shuai, B.; Liu, J.; and Wang, G. 2017. Deep level sets for salient object detection. In *Proceedings of the IEEE/CVF Conference on Computer Vision and Pattern Recognition*, 2300–2309.
- Hu, Y.-T.; Chen, H.-S.; Hui, K.; Huang, J.-B.; and Schwing, A. G. 2019. SAIL-VOS: Semantic amodal instance level video object segmentation—a synthetic dataset and baselines. In *Proceedings of the IEEE/CVF Conference on Computer Vision and Pattern Recognition*, 3105–3115.
- Johnson, B. A.; and Ma, L. 2020. Image segmentation and object-based image analysis for environmental monitoring: Recent areas of interest, researchers’ views on the future priorities.
- Kass, M.; Witkin, A.; and Terzopoulos, D. 1988. Snakes: Active contour models. *International journal of computer vision*, 1(4): 321–331.
- Ke, L.; Tai, Y.-W.; and Tang, C.-K. 2021. Deep occlusion-aware instance segmentation with overlapping bilayers. In *Proceedings of the IEEE/CVF conference on computer vision and pattern recognition*, 4019–4028.
- Ke, L.; Ye, M.; Danelljan, M.; Tai, Y.-W.; Tang, C.-K.; Yu, F.; et al. 2024. Segment anything in high quality. In *Advances in Neural Information Processing Systems*, volume 36.
- Kim, B.; and Ye, J. C. 2019. Mumford–Shah loss functional for image segmentation with deep learning. *IEEE transactions on image processing*, 29: 1856–1866.
- Kirillov, A.; Mintun, E.; Ravi, N.; Mao, H.; Rolland, C.; Gustafson, L.; Xiao, T.; Whitehead, S.; Berg, A. C.; Lo, W.-Y.; et al. 2023. Segment Anything. In *Proceedings of the IEEE/CVF International Conference on Computer Vision*, 4015–4026.
- Li, C.; Xu, C.; Gui, C.; and Fox, M. D. 2010a. Distance regularized level set evolution and its application to image segmentation. *IEEE transactions on image processing*, 19(12): 3243–3254.
- Li, K.; and Malik, J. 2016. Amodal instance segmentation. In *Proceedings of the IEEE/CVF European Conference on Computer Vision*, 677–693. Springer.
- Li, P.; Guo, J.; Song, B.; and Xiao, X. 2010b. A multilevel hierarchical image segmentation method for urban impervious surface mapping using very high resolution imagery. *IEEE Journal of Selected Topics in Applied Earth Observations and Remote Sensing*, 4(1): 103–116.
- Li, W.; Liu, W.; Zhu, J.; Cui, M.; Hua, X.-S.; and Zhang, L. 2022a. Box-supervised instance segmentation with level set evolution. In *European conference on computer vision*, 1–18. Springer.
- Li, Z.; Shi, R.; Huang, T.; and Jiang, T. 2023a. OAFormer: Learning occlusion distinguishable feature for amodal instance segmentation. In *International Conference on Acoustics, Speech, and Signal Processing*, 1–5. IEEE.
- Li, Z.; Ye, W.; Jiang, T.; and Huang, T. 2022b. 2D amodal instance segmentation guided by 3D shape prior. In *Proceedings of the IEEE/CVF European Conference on Computer Vision*, 165–181. Springer.
- Li, Z.; Ye, W.; Jiang, T.; and Huang, T. 2023b. GIN: Generative invariant shape prior for amodal instance segmentation. *IEEE Transactions on Multimedia*.
- Li, Z.; Ye, W.; Terven, J.; Bennett, Z.; Zheng, Y.; Jiang, T.; and Huang, T. 2023c. MUVA: A new large-scale benchmark for multi-view amodal instance segmentation in the shopping scenario. In *Proceedings of the IEEE/CVF International Conference on Computer Vision*, 23504–23513.

- Li, Z.; Yoon, H.; Lee, S.; and Lin, W. 2025. Unveiling the Invisible: Reasoning Complex Occlusions Amodally with AURA. In *Proceedings of the IEEE/CVF International Conference on Computer Vision*.
- Lin, T.-Y.; Maire, M.; Belongie, S.; Hays, J.; Perona, P.; Ramanan, D.; Dollár, P.; and Zitnick, C. L. 2014. Microsoft coco: Common objects in context. In *Proceedings of the IEEE/CVF European Conference on Computer Vision*, 740–755. Springer.
- Ling, H.; Acuna, D.; Kreis, K.; Kim, S. W.; and Fidler, S. 2020. Variational amodal object completion. *Advances in Neural Information Processing Systems*, 33: 16246–16257.
- Liu, Z.; Li, Z.; and Jiang, T. 2024. BLADE: Box-Level Supervised Amodal Segmentation through Directed Expansion. *Proceedings of the AAAI Conference on Artificial Intelligence*.
- Liu, Z.; Qiao, L.; Chu, X.; Ma, L.; and Jiang, T. 2025. Towards Efficient Foundation Model for Zero-shot Amodal Segmentation. In *Proceedings of the IEEE/CVF Conference on Computer Vision and Pattern Recognition*, 20254–20264.
- Malladi, R.; Sethian, J. A.; and Vemuri, B. C. 2002. Shape modeling with front propagation: A level set approach. *IEEE transactions on pattern analysis and machine intelligence*, 17(2): 158–175.
- Mas, J.-F.; and González, R. 2015. Change detection and land use/land cover database updating using image segmentation, GIS analysis and visual interpretation. *The International Archives of the Photogrammetry, Remote Sensing and Spatial Information Sciences*, 40: 61–65.
- Ngo, T. A.; and Carneiro, G. 2013. Left ventricle segmentation from cardiac MRI combining level set methods with deep belief networks. In *IEEE International Conference on Image Processing*, 695–699. IEEE.
- Nguyen, K.; and Todorovic, S. 2021. A weakly supervised amodal segmenter with boundary uncertainty estimation. In *Proceedings of the IEEE/CVF International Conference on Computer Vision*, 7396–7405.
- Ozguroglu, E.; Liu, R.; Surís, D.; Chen, D.; Dave, A.; Tokmakov, P.; and Vondrick, C. 2024. pix2gestalt: Amodal Segmentation by Synthesizing Wholes. *Proceedings of the IEEE/CVF Conference on Computer Vision and Pattern Recognition*.
- Paszke, A.; Gross, S.; Massa, F.; Lerer, A.; Bradbury, J.; Chanan, G.; Killeen, T.; Lin, Z.; Gimelshein, N.; Antiga, L.; et al. 2019. Pytorch: An imperative style, high-performance deep learning library. *Advances in Neural Information Processing Systems*, 32.
- Podell, D.; English, Z.; Lacey, K.; Blattmann, A.; Dockhorn, T.; Müller, J.; Penna, J.; and Rombach, R. 2024. Sdxl: Improving latent diffusion models for high-resolution image synthesis. *International Conference on Learning Representations*.
- Qi, L.; Jiang, L.; Liu, S.; Shen, X.; and Jia, J. 2019. Amodal instance segmentation with KINS dataset. In *Proceedings of the IEEE/CVF Conference on Computer Vision and Pattern Recognition*, 3014–3023.
- Ravi, N.; Gabeur, V.; Hu, Y.-T.; Hu, R.; Ryali, C.; Ma, T.; Khedr, H.; Rädle, R.; Rolland, C.; Gustafson, L.; et al. 2024. Sam 2: Segment anything in images and videos. *arXiv preprint arXiv:2408.00714*.
- Tai, W.-E.; Shih, Y.-L.; Sun, C.; Wang, Y.-C. F.; and Chen, H.-T. 2025. Segment Anything, Even Occluded. In *Proceedings of the IEEE/CVF Conference on Computer Vision and Pattern Recognition*, 29385–29394.
- Tang, M.; Valipour, S.; Zhang, Z.; Cobzas, D.; and Jagersand, M. 2017. A deep level set method for image segmentation. In *International Workshop on Deep Learning in Medical Image Analysis*, 126–134. Springer.
- Tran, M.; Bounsavy, W.; Vo, K.; Nguyen, A.; Nguyen, T.; and Le, N. 2024. ShapeFormer: Shape Prior Visible-to-Amodal Transformer-based Amodal Instance Segmentation. *arXiv preprint arXiv:2403.11376*.
- Tran, M.; Vo, K.; Yamazaki, K.; Fernandes, A.; Kidd, M.; and Le, N. 2022. Aisformer: Amodal instance segmentation with transformer. *British Machine Vision Conference*.
- Wang, Z.; Acuna, D.; Ling, H.; Kar, A.; and Fidler, S. 2019. Object instance annotation with deep extreme level set evolution. In *Proceedings of the IEEE/CVF Conference on Computer Vision and Pattern Recognition*, 7500–7508.
- Xiao, Y.; Xu, Y.; Zhong, Z.; Luo, W.; Li, J.; and Gao, S. 2021. Amodal segmentation based on visible region segmentation and shape prior. In *Proceedings of the AAAI Conference on Artificial Intelligence*, 4, 2995–3003.
- Xiong, Y.; Varadarajan, B.; Wu, L.; Xiang, X.; Xiao, F.; Zhu, C.; Dai, X.; Wang, D.; Sun, F.; Iandola, F.; et al. 2024. EfficientSAM: Leveraged masked image pretraining for efficient segment anything. In *Proceedings of the IEEE/CVF Conference on Computer Vision and Pattern Recognition*, 16111–16121.
- Zhan, G.; Zheng, C.; Xie, W.; and Zisserman, A. 2024. Amodal Ground Truth and Completion in the Wild. *Proceedings of the IEEE/CVF Conference on Computer Vision and Pattern Recognition*.
- Zhan, X.; Pan, X.; Dai, B.; Liu, Z.; Lin, D.; and Loy, C. C. 2020. Self-supervised scene de-occlusion. In *Proceedings of the IEEE/CVF Conference on Computer Vision and Pattern Recognition*, 3784–3792.
- Zhang, Z.; Chen, A.; Xie, L.; Yu, J.; and Gao, S. 2019. Learning semantics-aware distance map with semantics layering network for amodal instance segmentation. In *ACM International Conference on Multimedia*, 2124–2132.
- Zhao, Y.; Shanguan, Z.; Fan, W.; Cao, Z.; and Wang, J. 2020. U-net for satellite image segmentation: Improving the weather forecasting. In *2020 5th International Conference on Universal Village (UV)*, 1–6. IEEE.
- Zheng, C.; Dao, D.-S.; Song, G.; Cham, T.-J.; and Cai, J. 2021. Visiting the invisible: Layer-by-layer completed scene decomposition. *International Journal of Computer Vision*, 129: 3195–3215.